Electronic and optical properties of ZnO quantum dots under hydrostatic pressure

Zaiping Zeng,[1] Christos S. Garoufalis,[1,2] Sotirios Baskoutas,[1,*] and Gabriel Bester[3,†]

[1]*Materials Science Department, University of Patras, 26504 Patras, Greece*
[2]*Department of Environment Technology and Ecology, Technological Institute of Ionian Islands, 2 Kalvou Square, 29100 Zakynthos, Greece*
[3]*Max-Planck-Institut für Festkörperforschung, D-70569 Stuttgart, Germany*

In the present work, we studied the electronic and optical properties of ZnO quantum dots (QDs) subjected to externally applied hydrostatic pressure. Our single-particle calculations are based on the empirical pseudopotential method and the excitonic effects are considered by employing the configuration interaction approach. The optical band gap, Stokes shift, and optical emission polarization have been investigated as a function of the applied pressure. It is found that the applied pressure causes a linear increase in the optical band gap. The pressure coefficient appears to be highly size dependent, exhibiting a monotonic increase with increasing QD size. In contrast to this monotonic behavior, the applied pressure induces a nonmonotonic Stokes shift which presents a minimum value at a critical pressure. For pressures larger than this critical value, the optical emission polarization exhibits a sharp transition from in-plane to out-of-plane polarization. Finally, it is found that the critical pressure at which the crossing takes place strongly depends on the QD size, showing larger values for larger QD sizes. Beyond this crossing point, the lowest optically bright exciton state mainly originates from one Slater determinant, where both the single-particle electron and hole states have an *S*-type envelope function and the hole state originates mainly from the bulk Bloch C band.

PACS number(s): 78.67.Hc, 73.21.La, 73.22.Dj, 73.22.Lp

I. INTRODUCTION

Nanostructures and heterostructures made of zinc oxide (ZnO), such as nanowalls,[1] nanotubes,[2] nanorods,[3] and quantum dots (QDs),[4] have already been used as transparent conductors in solar cells and as components in high-power electronics, UV light emitters, and gas and chemical sensors (see Ref. [5] and references therein). Possible applications of ZnO nanostructures in optoelectronic and spintronic devices, such as laser diodes with polarized output, and spin-based memory and logic, have also attracted great attention.[6,7] As an important member of the nanostructure family, zero-dimensional ZnO QDs have become the subject of recent developments. Experimental fabrication of this type of nanostructure has been achieved by using different chemical synthesis methods, such as sol-gel,[8] thermolysis,[9] and polyol methods,[4] to mention only a few. From a theoretical point of view, due to the specifics of the wurtzite ZnO material, such as the anisotropy of the valence band, as well as the small dielectric constant and correspondingly strong electron-hole Coulomb interaction, simple one-band effective-mass models fail to deliver predictive results. To have a good interpretation of experimental measurements and optimization of ZnO QDs for possible device applications, an accurate theoretical method able to predict the transition energy and the oscillator strength of optical transitions is required. Accurate atomistic empirical pseudopotential calculations have been shown to describe exciton states in CdSe QDs (Ref. [10]), and very recently in ZnO QDs,[11] very well.

On the other hand, high-pressure investigations of semiconductor nanostructures such as nanocrystals or QDs have emerged as a focus area in condensed-matter physics and material science because of their large impact on the tunable optical properties that may be advantageous for application in optoelectronics, QD lasers, high-density memory, bioengineering, etc.[12–15] Most of the existing theoretical work

concerning the hydrostatic pressure effect focused on QDs with zinc-blende structure, such as self-assembled InAs/GaAs (Ref. [16]) or InGaAs/GaAs (Ref. [17]) QDs. Theoretical work associated with the pressure effect in wurtzite ZnO colloidal QDs is very limited.[18] Here, we study the electronic and optical properties of ZnO QDs under externally applied hydrostatic pressure. The single-particle orbitals and energies are calculated by the atomistic empirical pseudopotential method using recently derived pseudopotentials,[11] considering the effects of multiband coupling, multivalley coupling, and spin-orbit interaction, while the excitonic effects are taken into account by using the configuration interaction approach.[19] The present numerical results cover a variety of optical properties of ZnO QDs under pressure, such as the optical band gap, the pressure coefficient, the Stokes shift, and the optical emission polarization.

In the following section, we outline the computational details. Thereafter, in Sec. III numerical results and related discussions are presented. Sec. IV is devoted to conclusions.

II. COMPUTATIONAL DETAILS

The single-particle energies and eigenstates for both conduction and valence bands are obtained by the plane-wave empirical pseudopotential method,[20] using our recently derived ZnO pseudopotentials.[11] The adopted Hamiltonian for the single-particle states has the form

$$\widehat{H} = -\frac{1}{2}\nabla^2 + \sum_{n\alpha}\left[v_\alpha(|\vec{r} - \vec{R}_{\alpha n}|;\epsilon) + \widehat{v}_\alpha^{SO}\right], \quad (1)$$

where n is an atomic index, α specifies the atom type, and $\widehat{v}_\alpha^{SO}$ is the nonlocal spin-orbit operator. The screened atomic pseudopotentials v_α (with α = Zn, O) are centered at each atomic position and their superposition generates the crystal potential. These pseudopotentials v_α incorporate
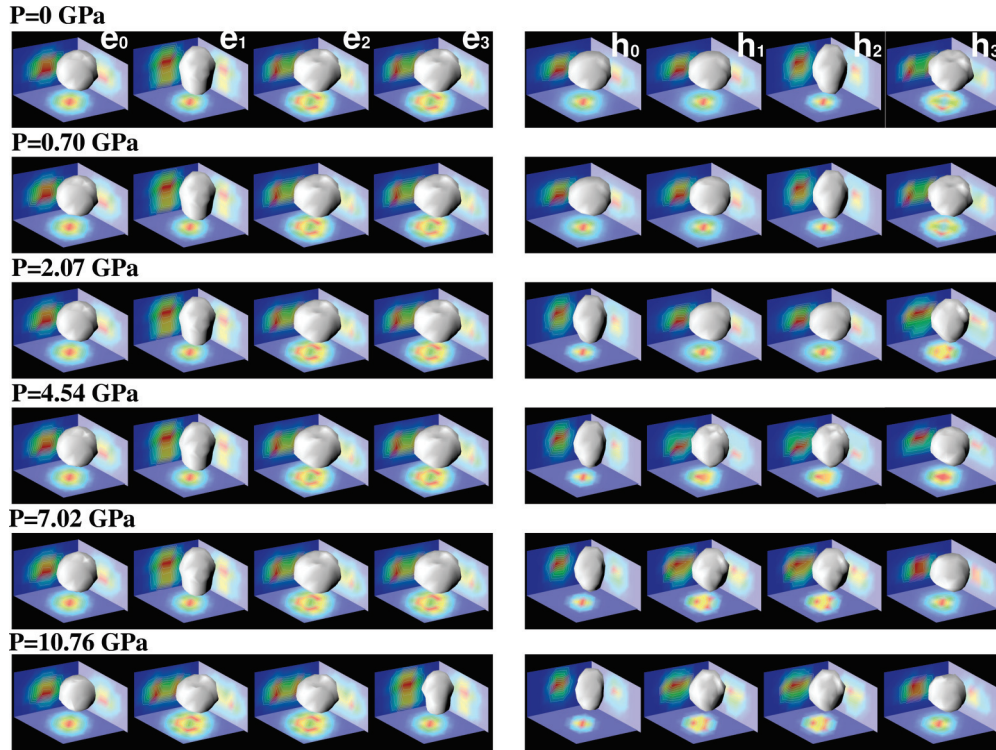
FIG. 1. (Color online) Envelope functions for the first four electron ($e_{0,1,2,3}$) and first four hole ($h_{0,1,2,3}$) states in a ZnO QD with diameter D = 1.7 nm for various hydrostatic pressures. The isosurface values are chosen in such a way to enclose 75% of the state densities.

the dependence on the local hydrostatic strain $\mathrm{Tr}(\epsilon)$ via the relationship[21]

$$v_\alpha(r;\epsilon) = v_\alpha^{\mathrm{eq}}(r;0)[1 + \gamma_\alpha \mathrm{Tr}(\epsilon)], \tag{2}$$

where γ_α is a fitting parameter. The form and the parameters of the zero strain potential, which are optimized to reproduce the known band structure and the bulk properties of ZnO, are given in Ref. 11. In our calculations, the fitting parameter γ_α has the value 0.304, giving a pressure coefficient for bulk ZnO equal to 24.7 meV/GPa, which is in very good agreement with the experimental value of 24.7 ± 0.1 meV/GPa.[22] This also gives the conduction and valence band deformation potentials[17]
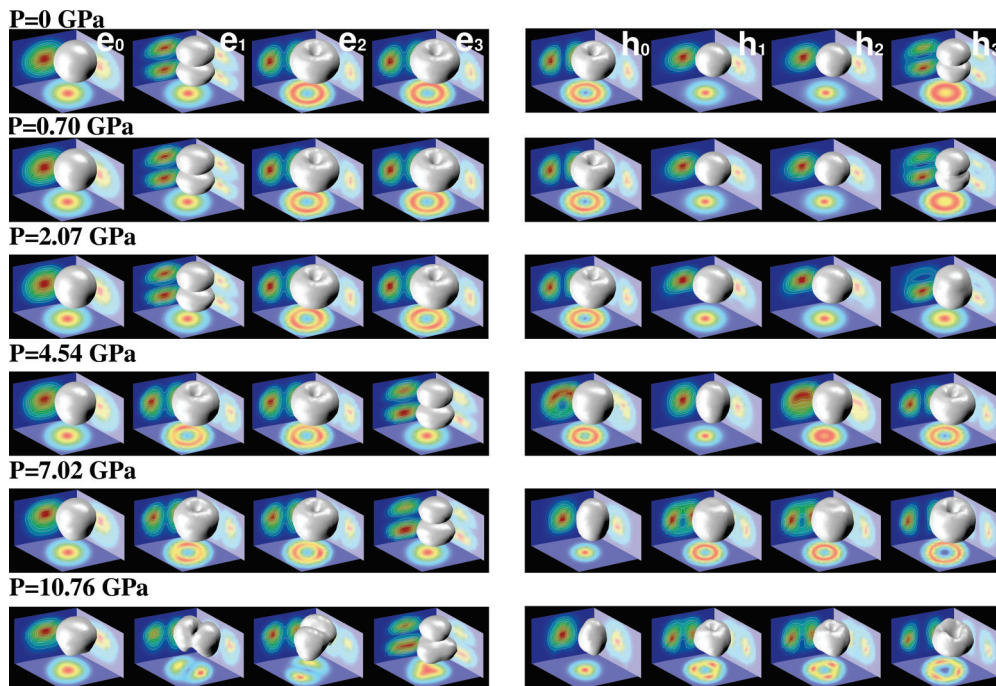

FIG. 2. (Color online) Same as Fig. 1 but for D = 5.2 nm.

$a_c = -4.65$ eV and $a_v = -2.54$ eV, respectively, resulting in a (relative) band-gap deformation potential $a_g = -2.11$ eV, which agrees fairly well with the results predicted by the local-density approximation (LDA) and the LDA $+ U$ (Ref. [23]): $a_g = -1.7$ eV (LDA) and $a_g = -2.9$ eV (LDA $+ U$). The experimental value of the effective deformation potential for bulk ZnO is ~ -3.51 to -3.81 eV, and -3.5 ± 0.4 eV obtained by different experimental methods.[24,25] The pressure values used in our calculations are determined approximately by using the Murnaghan equation of state[17,26]

$$P = (B/B')[(V_0/V)^{B'} - 1], \qquad (3)$$

taking for the wurtzite ZnO bulk modulus $B = 142.4$ GPa and for the pressure derivative $B' = dB/dP = 3.6$.[22]

The surface passivation is approximated by a high-band-gap artificial material, as practiced successfully previously.[11,27,28] The structure was relaxed with Keating's valence force field (VFF) model for wurtzite materials.[29] It should be noted that the VFF relaxed structures exhibit a qualitatively correct variation of c/a and u internal parameters with respect to pressure (i.e., c/a decreases while u increases when the pressure increases[30,31]). The corresponding envelope functions of the single-particle states in both valence and conduction bands are obtained by projecting the fast-oscillating atomic wave functions onto the Bloch states of each unit cell [according to Eq. (6) of Ref. [11]]. This effectively smears out the atomic oscillations and leads to an envelope function that can be displayed with clarity.[11,27] This procedure also allows us to obtain the Bloch function character of each QD state and analyze them in terms of their Bloch function parentage: A, B, or C band (or a mixture of them). The excitonic wave functions are expanded in terms of single-substitution Slater determinants constructed from the single-particle wave functions of electrons and holes. The corresponding many-body Hamiltonian is solved using iterative diagonalization techniques. Our computational limitations allow us to include in the configuration interaction (CI) treatment ten states from the valence band and ten states from the conduction band. For the screening function needed in the Coulomb integrals we used the phenomenological microscopic, isotropic, and uniform model proposed by Resta.[32] The optical dipole matrix elements are calculated within the dipole approximation, and the oscillator strength was calculated using Fermi's golden rule. A review of this method can be found in Ref. [33].

III. RESULTS AND DISCUSSION

A. Pressure-dependent electronic properties

To determine the electronic and optical properties in ZnO QDs in both the strong and the intermediate confinement regime under externally applied hydrostatic pressure, we considered five different ZnO colloidal QDs with diameters $D = 1.7, 2.1, 3.1, 3.6,$ and 5.2 nm, respectively. ZnO QDs with such sizes can be experimentally synthesized by using the well-established colloidal fabrication techniques, leading to a nearly spherical shape.[4,8] The numbers of atoms for the respective structures are $Zn_{99}O_{111}$, $Zn_{204}O_{210}$, $Zn_{654}O_{654}$, $Zn_{1014}O_{1011}$, and $Zn_{3063}O_{3102}$.

TABLE I. Character of the first four envelope functions for electrons and holes in a ZnO QD with diameter $D = 1.7$ nm under various hydrostatic pressures (in unit of GPa). The superscript (A, B, C) indicates the corresponding hole-state parentage (A, B, or C band) obtained from Fig. 3 and the asterisk means that the wave function is a mixed state with orbital P character.

Pressure	e_0	e_1	e_2	e_3	h_0	h_1	h_2	h_3
0	S	P_z	P_{xy}	P_{xy}	S^A	S^B	S^C	P_{xy}^{AB}
0.70	S	P_z	P_{xy}	P_{xy}	S^A	S^B	S^C	P_{xy}^{AB}
2.07	S	P_z	P_{xy}	P_{xy}	S^{C*}	S^{A*}	S^{B*}	S^{C*}
4.54	S	P_z	P_{xy}	P_{xy}	S^{C*}	S^{AC*}	S^{BC*}	S^{ABC*}
7.02	S	P_z	P_{xy}	P_{xy}	S^C	P_{xy}^C	P_{xy}^C	S^A
10.76	S	P_{xy}	P_{xy}	P_z	S^C	P_{xy}^C	P_{xy}^C	S^A

As a first step toward elucidating the electronic structure in ZnO QDs, we project the fast-oscillating atomic wave functions onto the bulk ZnO Bloch states (as stated in Sec. II). This gives us access to the envelope functions, which are more convenient to visualize than the fast-oscillating real wave functions. However, it should be kept in mind that the energetics for each state is not governed by the envelope function alone, but determined by the full atomic wave function. As the representatives of the electronics of ZnO QDs under hydrostatic pressure in both the strong and intermediate confinement regimes, we present the projected envelope functions of the first four electron states and the first four hole states of our smallest and largest structures in Figs. 1 and 2, respectively. The figures show results for six different hydrostatic pressures. To characterize the symmetry of the wave functions, which is very useful to understand the relevant optical properties discussed in the next section, we use the notation ω_ζ, where ω represents the number of nodes encountered by moving across a specific direction (xy or z-axis direction), while the subscript ζ indicates the direction in which we find the node(s). The possible value for ω are S, P, D, etc., where S represents the form of the wave function without node (in this case, we neglect the subscript ζ), P with one node, etc. This way, we tabulated the characters of the electron and hole envelope functions shown in Figs. 1 and 2 in Tables I and II, respectively.

In Fig. 3 we plot the Bloch function character of the first four hole states using the projection formalism described in Sec. II. After a combined analysis of the relative contribution from the bulk valence bands with the characters of the hole envelope functions listed in Tables I and II, we find that, in the absence of external pressure, the highest occupied molecular orbital

TABLE II. Same as Table I but for $D = 5.2$ nm.

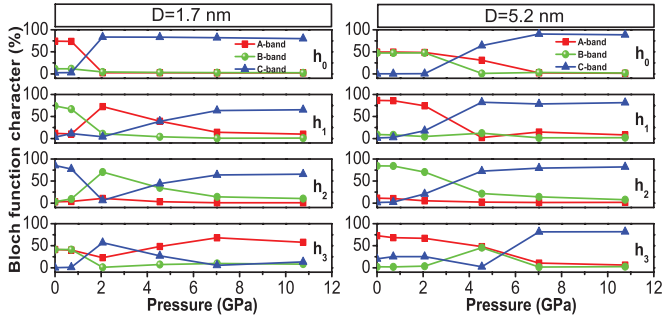| Pressure	e_0	e_1	e_2	e_3	h_0	h_1	h_2	h_3
0	S	P_z	P_{xy}	P_{xy}	P_{xy}^{AB}	S^A	S^B	P_z^A
0.70	S	P_z	P_{xy}	P_{xy}	P_{xy}^{AB}	S^A	S^B	P_z^A
2.07	S	P_z	P_{xy}	P_{xy}	P_{xy}^{AB}	S^A	S^B	P_z^A
4.54	S	P_{xy}	P_{xy}	P_z	P_{xy}^{ABC}	S^C	S^C	P_{xy}^{AB}
7.02	S	P_{xy}	P_{xy}	P_z	S^C	P_{xy}^C	P_{xy}^C	P_{xy}^C
10.76	S	P_y	P_x	P_z	S^C	P_{xy}^C	P_{xy}^C	P_{xy}^C

FIG. 3. (Color online) Analysis of the Bloch function character of the first four hole states $h_{0,1,2,3}$ in a ZnO QD under various hydrostatic pressures. The left-hand panel corresponds to the QD with diameter $D = 1.7$ nm, while the right-hand panel corresponds to the QD with diameter $D = 5.2$ nm. The colors red, green, and blue correspond to A, B, and C bands, respectively.
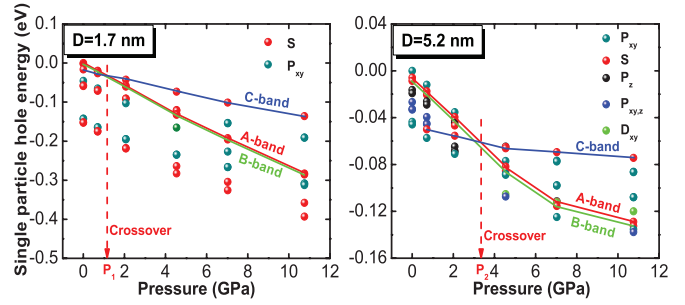

FIG. 4. (Color online) Energy of the first ten hole states relative to the HOMO state at zero pressure, in ZnO QDs under various hydrostatic pressures (in units of GPa). The lines connect states which are of the same symmetry ω_ζ. The red, green, and blue lines connect states with dominant A-, B-, and C-band character, respectively. Two QD sizes, $D = 1.7$ and 5.2 nm, where D is the diameter of the QD, are considered.

(HOMO, h_0) of our smallest structure (with diameter $D = 1.7$ nm) has orbital S character, while it shows a P character in our largest structure (with diameter $D = 5.2$ nm). This is in agreement with one of the important conclusions of Ref. 11 which demonstrates that the HOMO of ZnO QDs is of orbital P character for structures larger than 2.6 nm in diameter. Under pressure, the orbital character of the HOMO state of our smallest structure appears to be pressure independent, always exhibiting a conventional S-type character. Conversely, the orbital character of the HOMO state of our largest structure experiences a drastic change in the envelope function character, switching to a more conventional S orbital character for pressures larger than 2.07 GPa. This is due to the pressure effect which modifies the Bloch function parentage from an even mixture of A and B bands ($P \leqslant 2.07$ GPa) to a nearly pure single C band ($P > 2.07$ GPa), as seen in Fig. 3 (see the top plot of the right-hand panel). In addition to the HOMO state, the applied pressure significantly modifies the Bloch function characters for the other hole states ($h_{1,2,3}$): they are nearly pure single-band objects for relatively high pressures (e.g., $P > 4.54$ GPa), originating mainly from the bulk Bloch C band ($\sim$75%) and exhibiting P_{xy}-type characters. The only exception is h_3 of our smallest structure, which has a dominant bulk Bloch A-band parentage and shows an S-type character for pressures larger than 4.54 GPa. The fact that the P_{xy}^C states at the pressures of 7.02 and 10.76 GPa ($h_{1,2}$ states in Table I) are energetically separated from the P_z^C state can be related to the anisotropic effective masses of the topmost three ZnO valence bands. The C-band effective mass is anisotropic and larger perpendicular to the c axis ($m_{C\perp}^* = 0.55 m_0$ and $m_{C\parallel}^* = 0.31 m_0$, where m_0 is the free electron mass). This favors the orbital P states with in-plane nodes, P_{xy}, over the ones with nodes along the c axis, P_z. No such anisotropy exists for the A and B bands, and the orbital P_{xy} states are not favored over the P_z states. The electron states follow the typical pattern of a single-band object originating from an isotropic band. The lowest four electron states have orbital S and P character, where P_z is slightly favored over P_{xy} at low pressures and vice versa at high pressures.

As mentioned before, the applied hydrostatic pressure strongly modifies the relative contribution of the bulk valence band states to the QD hole states, which causes the changes

in the symmetry of the hole envelope functions. In Fig. 4, we see that states with dominant A- and B-band parentage have a stronger dependence on pressure than the states with dominant C-band parentage. This is associated with the larger deformation potential of A and B bands in comparison to that of the C band. Figure 4 also shows that the C-band states rise above the A- and B-band states at a critical pressure and finally become the energetically favorable states. This critical pressure appears to be highly size dependent. For our smallest structure, it is $P_1 \approx 1.2$ GPa, while for our largest structure, it is $P_2 \approx 3.3$ GPa.

B. Pressure-dependent optical properties

We first present the optical band gap of ZnO QDs as a function of the applied hydrostatic pressure. The calculations are performed for five different QD sizes which are in the strong or intermediate confinement regime. Two levels of theory, at the single-particle (SP) level and at the CI level, are employed. Figures 5(a) and 5(b) show a strong size dependence of the optical band gap and a weaker, nearly linear, pressure dependence. The pressure coefficients (dE/dP) are given in Fig. 5(c) for uncorrelated and correlated calculations. Both the single-particle and the excitonic pressure coefficients are strongly size dependent. Increasing the QD size causes a monotonic increase in the pressure coefficient. A similar behavior has also been calculated theoretically for CdSe QDs.[34] Furthermore, it is shown from Fig. 5(c) that the QD excitonic pressure coefficients obtained in the full CI scheme are substantially smaller than the bulk value (see the dot-dashed line), with deviations at small diameters of up to 41%. The single-particle results exceed the bulk limit for QD diameters larger than $D = 4.5$ nm. This prominently highlights the importance of the higher level of theory accounting for excitonic effects. We also studied in Fig. 5(d) the Stokes shift, defined as the energetic difference between the lowest dark exciton state and the first bright exciton state. The Stokes shift displays a nonmonotonic dependence of the applied hydrostatic pressure, exhibiting a minimum value at a critical pressure P_c. This critical pressure is highly size sensitive. It appears to be $P_c = 0.7$ GPa for the first two smallest structures, $P_c = 2.07$ GPa for the QD diameter
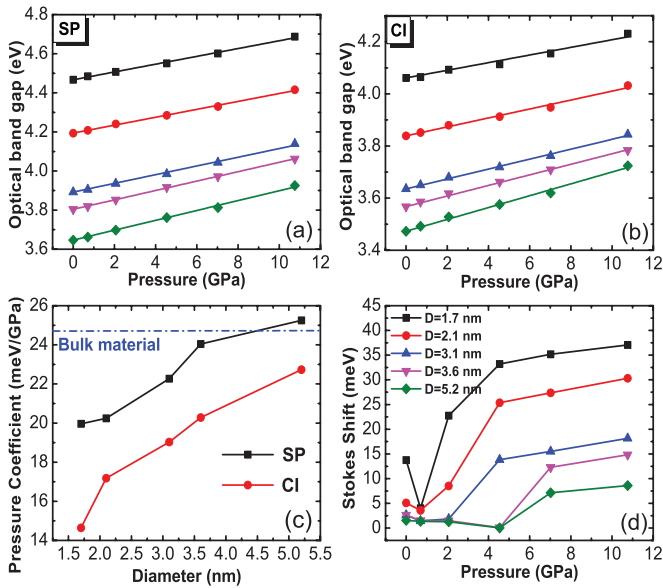
FIG. 5. (Color online) Optical band gap of ZnO QDs at (a) the single-particle (SP) level and (b) the CI level as a function of the hydrostatic pressure (symbols). (c) Pressure coefficients at the single-particle level [obtained from (a) and at the CI level [obtained from (b)] versus QD diameter. (d) Stokes shift as a function of the applied hydrostatic pressures. Here, five different QD sizes ($D = 1.7$, 2.1, 3.1, 3.6, and 5.2 nm, where D is the QD diameter) are considered. All the symbols and colors in (a) and (b) are the same as in (d).

$D = 3.1$ nm, and $P_c = 4.54$ GPa for the other two largest structures.

To clarify the physical reasons for this nonmonotonic behavior, we take our largest structure as an example and recall the electronic properties of the single electron and hole states presented in the previous section. For pressures smaller than or equal to the critical value ($P = 4.54$ GPa), both the first bright and dark exciton states have a dominant contribution from the $(0,1)$ configuration, where both the electron and the hole

have S-type orbital character. In the CI scheme, the lowest exciton state is spin forbidden. However, when the applied pressure is larger than the critical value ($P > 4.54$ GPa), the single-particle states which are responsible for the two exciton states show an abrupt change from the configuration $(0,1)$ to the configuration $(0,0)$. This level crossing is responsible for the nonmonotonic behavior in the Stokes shift. This nonmonotonic behavior in the Stokes shift makes evident that the electron-hole spin-exchange interaction is much stronger in the $(0,0)$ configuration (C exciton) and it is enhanced with increasing pressure. Similar behavior has also been experimentally measured and theoretically calculated in CdSe nanorods by systematically varying the height-to-diameter aspect ratio.[35] For larger pressures, Fig. 5(d) shows that the Stokes shift is significantly larger than the corresponding value at zero pressure. A larger Stokes shift means a smaller overlap area between absorption and emission spectra, which is desirable in applications such as light-emitting diodes, where reabsorption reduces the total efficiency.[35]

Finally, we calculate in Fig. 6 the photoluminescence emission spectrum in the full CI scheme for our smallest and largest structures. We find that the applied pressure induces a strong blueshift in the emission spectrum. This blueshift is more pronounced in the larger QD in accordance with Fig. 5(c). In an attempt to indicate explicitly the emission polarization direction, we also present the spectra at each pressure with a vertical line. It is shown that, in both the strong and intermediate confinement regimes, the optical emission polarization exhibits a crossing from in-plane ($\mathbf{E} \perp \vec{c}$) to out-of-plane ($\mathbf{E} \parallel \vec{c}$) polarization at a critical pressure value. It is $P_c = 0.70$ GPa for our smallest structure and $P_c = 4.54$ GPa for our largest structure. In other words, the emission changes from a normal α emission ($\mathbf{E} \perp \vec{c}$) to the unusual[36,37] so-called σ and π emissions ($\mathbf{E} \parallel \vec{c}$) for pressures larger than the critical pressure. After reaching the crossing, the lowest optically bright exciton state in both confinement regimes has a dominant contribution from the $(0,0)$ configuration, where the single-particle hole state has S-type character and is derived
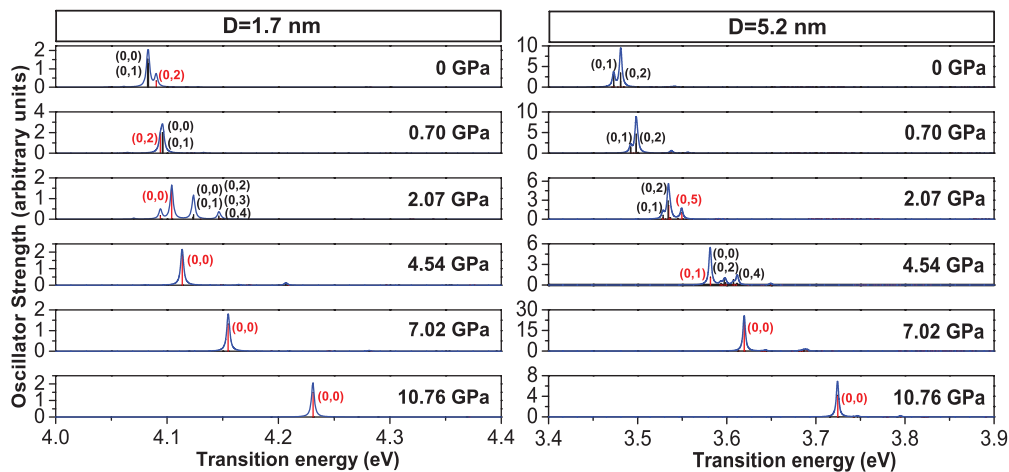

FIG. 6. (Color online) Oscillator strength for the emission $|X\rangle$ to $|0\rangle$ at room temperature in ZnO QDs, which are obtained by full CI. Transitions polarized along the out-of-plane direction (c axis) are shown by red vertical lines, while the ones polarized along the in-plane direction are shown as black vertical lines. The numbers in parentheses refer to the dominant single-particle levels involved in the transitions (e,h). The blue curve represents the total emission spectra. The left-hand panel corresponds to the QD with diameter $D = 1.7$ nm, while the right-hand panel corresponds to the QD with diameter $D = 5.2$ nm.

from the dominant bulk Bloch C-band contribution. Recently, it has been shown that the polarization of the C exciton along the c axis ($\mathbf{E}\|\vec{c}$) holds not only for bulk ZnO (Ref. 38) but also for ZnO nanowires.[39] The possibility to effectively manipulate the optical emission polarization of QDs via pressure should be advantageous in the design of future experiments.

IV. CONCLUSIONS

In summary, we studied the electronic and optical properties of ZnO colloidal QDs as a function of applied hydrostatic pressure. We find that for QD larger than 2.6 nm in diameter, the increased pressure induces a drastic change in the highest occupied molecular orbital from an unconventional P-type character to a normal S-type character. Hole states tend to become single-band objects originating from the Bloch C band with increasing pressure. We relate this effect to the fact that the hole states with dominant A- and B-band parentage experience a stronger pressure dependence, in comparison to the corresponding C-band states. In other words, the Bloch band hydrostatic deformation potentials are negative and larger in magnitude for the A or B bands than for the C band. As a consequence, the C-band states emerge as the HOMO states at high pressure. We show that the crossover between A- or B-band and C-band HOMO states is size dependent and occurs at higher pressures for larger QDs. We further find that the P states derived from the Bloch C band are energetically split into states with nodes in plane and nodes along the c direction. This is attributed to the anisotropy of the bulk Bloch C band, which has a heavier in-plane effective mass favoring P states with in-plane nodes. At both the single-particle level and the correlated excitonic level, the optical band gap experiences a linear increase with increasing pressure, with a highly size-dependent pressure coefficient. The pressure coefficient is significantly lowered, by as much as 41%, by correlations. Only the correlated results (configuration interaction) can be brought into agreement with experiment. In contrast to the monotonic increase of the optical band gap, the applied hydrostatic pressure causes a nonmonotonic Stokes shift with a minimum at a specific pressure. For pressures larger than this critical value, the optical emission polarization changes from in-plane to out-of-plane polarization. We explained this behavior through the drastic change of the single-particle hole state parentage from a dominant bulk Bloch A or B band (before crossing) to a nearly pure C band (after crossing). Finally, we find that the critical pressure at which the crossing takes place strongly depends on the QD size, showing larger pressure values for larger QD sizes. After this crossing, the optically bright exciton state has a pure contribution from the (0,0) configuration, where both the electron and hole states have S-type orbital character and the single-particle hole state has a dominant contribution from the bulk Bloch C band.

*Corresponding author: bask@upatras.gr

†Corresponding author: G.Bester@fkf.mpg.de

[1] M. Q. Israr, J. R. Sadaf, O. Nur, M. Willander, S. Salman, and B. Danielsson, Appl. Phys. Lett. **98**, 253705 (2011).

[2] H. Guo, Z. Lin, Z. Feng, L. Lin, and J. Zhou, J. Phys. Chem. C **113**, 12546 (2009).

[3] S. H. Ko, D. Lee, H. W. Kang, K. H. Nam, J. Y. Yeo, S. J. Hong, C. P. Grigoropoulos, and H. J. Sung, Nano Lett. **11**, 666 (2011).

[4] N. Bouropoulos, I. Tsiaoussis, P. Poulopoulos, P. Roditis, and S. Baskoutas, Mater. Lett. **62**, 3533 (2008); Q. Qiao, B. Li, C. Shan, J. Liu, J. Yu, X. Xie, Z. Zhang, T. Ji, Y. Jia, and D. Shen, *ibid.* **74**, 104 (2012).

[5] A. Djurisic and Y. H. Leung, Small **2**, 944 (2006).

[6] U. Özgür, Y. I. Alivov, C. Liu, A. Teke, M. A. Reshchikov, S. Doğan, V. Avrutin, S.-J. Cho, and H. Morkoç, J. Appl. Phys. **98**, 041301 (2005).

[7] V. A. Fonoberov and A. A. Balandin, J. Nanoelectron. Optoelectron. **1**, 19 (2006).

[8] K.-F. Lin, H.-M. Cheng, H.-C. Hsu, L.-J. Lin, and W.-F. Hsieh, Chem. Phys. Lett. **409**, 208 (2005).

[9] M. Salavati-Niasari, F. Davar, and Z. Fereshteh, Chem. Eng. J. **146**, 498 (2009).

[10] M. Califano, A. Zunger, and A. Franceschetti, Nano Lett. **4**, 525 (2004).

[11] S. Baskoutas and G. Bester, J. Phys. Chem. C **114**, 9301 (2010).

[12] H. Fu and A. Zunger, Phys. Rev. Lett. **80**, 5397 (1998).

[13] S. J. Chen, Y. C. Liu, C. L. Shao, C. S. Xu, Y. X. Liu, C. Y. Liu, B. P. Zhang, L. Wang, B. B. Liu, and G. T. Zou, Appl. Phys. Lett. **88**, 133127 (2006).

[14] X. Michalet, F. F. Pinaud, L. A. Bentolila, J. M. Tsay, S. Doose, J. J. Li, G. Sundaresan, A. M. Wu, S. S. Gambhir, and S. Weiss, Science **307**, 538 (2005).

[15] G. Ouyang, C. Q. Sun, and W. G. Zhu, J. Phys. Chem. C **113**, 9516 (2009).

[16] J.-W. Luo, S.-S. Li, J.-B. Xia, and L.-W. Wang, Phys. Rev. B **71**, 245315 (2005).

[17] G. A. Narvaez, G. Bester, and A. Zunger, Phys. Rev. B **72**, 041307 (2005).

[18] J. W. Li, L. W. Yang, Z. F. Zhou, P. K. Chu, X. H. Wang, J. Zhou, L. T. Li, and C. Q. Sun, J. Phys. Chem. C **114**, 13370 (2010).

[19] A. Franceschetti, H. Fu, L. W. Wang, and A. Zunger, Phys. Rev. B **60**, 1819 (1999).

[20] L.-W. Wang and A. Zunger, J. Chem. Phys. **100**, 2394 (1994).

[21] A. J. Williamson, L. W. Wang, and A. Zunger, Phys. Rev. B **62**, 12963 (2000).

[22] H. Morkoç and U. Özgür, *Zinc Oxide* (Wiley-VCH, Weinheim, 2009).

[23] A. Janotti and C. G. Van de Walle, Phys. Rev. B **75**, 121201 (2007).

[24]A. Mang, K. Reimann, and S. Rübenacke, Solid State Commun. **94**, 251 (1995).

[25]A. Segura, J. A. Sans, F. J. Manjón, A. Muñoz, and M. J. Herrera-Cabrera, Appl. Phys. Lett. **83**, 278 (2003).

[26]B. Welber, M. Cardona, C. K. Kim, and S. Rodriguez, Phys. Rev. B **12**, 5729 (1975).

[27]S. Baskoutas and G. Bester, J. Phys. Chem. C **115**, 15862 (2011).

[28]M. Califano, G. Bester, and A. Zunger, Nano Lett. **3**, 1197 (2003).

[29]D. Camacho and Y. M. Niquet, Physica E **42**, 1361 (2010).

[30]L. Wang, H. Liu, J. Qian, W. Yang, and Y. Zhao, J. Phys. Chem. C **116**, 2074 (2012).

[31]Z. Dong, K. K. Zhuravlev, S. A. Morin, L. Li, S. Jin, and Y. Song, J. Phys. Chem. C **116**, 2102 (2012).

[32]R. Resta, Phys. Rev. B **16**, 2717 (1977).

[33]G. Bester, J. Phys: Condens. Matter **21**, 023202 (2009).

[34]C. D. Grant, J. C. Crowhurst, S. Hamel, A. J. Williamson, and N. Zaitseva, Small **4**, 788 (2008).

[35]J. Hu, L.-s. Li, W. Yang, L. Manna, L.-w. Wang, and A. P. Alivisatos, Science **292**, 2060 (2001).

[36]N. S. Han, H. S. Shim, S. Lee, S. M. Park, M. Y. Choi, and J. K. Song, Phys. Chem. Chem. Phys. **14**, 10556 (2012).

[37]Z. Fan, P. chun Chang, J. G. Lu, E. C. Walter, R. M. Penner, C. hung Lin, and H. P. Lee, Appl. Phys. Lett. **85**, 6128 (2004).

[38]J. Rowe, M. Cardona, and F. Pollak, Solid State Commun. **6**, 239 (1968).

[39]G. Jacopin, L. Rigutti, A. Bugallo, F. Julien, C. Baratto, E. Comini, M. Ferroni, and M. Tchernycheva, Nanoscale Res. Lett. **6**, 501 (2011).